Accepted Manuscript

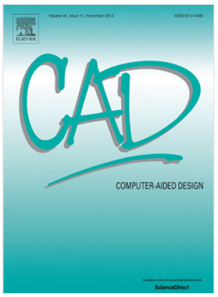

Optimal design and modeling of gyroid-based functionally graded cellular structures for additive manufacturing

Dawei Li, Wenhe Liao, Ning Dai, Guoying Dong, Yunlong Tang, Yi Min Xie

PII: S0010-4485(18)30038-1
DOI: https://doi.org/10.1016/j.cad.2018.06.003
Reference: JCAD 2628

To appear in: *Computer-Aided Design*

Received date : 26 January 2018
Accepted date : 23 June 2018

Please cite this article as: Li D., Liao W., Dai N., Dong G., Tang Y., Xie Y.M., et al. Optimal design and modeling of gyroid-based functionally graded cellular structures for additive manufacturing. *Computer-Aided Design* (2018), https://doi.org/10.1016/j.cad.2018.06.003

Optimal Design and Modeling of Gyroid-based Functionally Graded Cellular Structures for Additive Manufacturing

Dawei Li [a], Wenhe Liao [a], Ning Dai [*, a], Guoying Dong [b], Yunlong Tang [b], Yi Min Xie [c]

a. College of Mechanical and Electrical Engineering, Nanjing University of Aeronautics and Astronautics, Nanjing, 210016, China
b. Department of Mechanical Engineering, McGill University, Montreal, Quebec, H3A 0G4, Canada
c. Centre for Innovative Structures and Materials, School of Engineering, RMIT University, GPO Box 2476, Melbourne 3001, Victoria, Australia

* Corresponding authors.

Email addresses: davidlee@nuaa.edu.cn (D. Li) dai_ning@nuaa.edu.cn (N. Dai)

Abstract:

Lightweight cellular structure generation and topology optimization are common design methodologies in additive manufacturing. In this work, we present a novel optimization strategy for designing functionally graded cellular structures with desired mechanical properties. This approach is mainly by generating variable-density gyroid structure and then performing graded structure optimization. Firstly, the geometric properties of the original gyroid structures are analyzed, and the continuity and connectivity of the structures are optimized by adding a penalty function. Then, a homogenization method is used to obtain mechanical properties of gyroid-based cellular structures through a scaling law as a function of their relative densities. Secondly, the scaling law is added directly into the structure optimization algorithm to compute the optimal density distribution in part being optimized. Thirdly, the density mapping and interpolation approach are used to map the output of structure optimization into the parametric gyroid structure which results in an optimum lightweight lattice structure with uniformly varying densities across the design space. Lastly, the effectiveness and robustness of the optimized results are analyzed through finite element analysis and experiments.

Keywords:

Cellular Structure; Gyroid Structure; Functionally Graded Materials; Structure Optimization

1. Introduction

Additive manufacturing (AM) provides an opportunity to design and produce components with complex shape and topology [1]. However, current design for manufacturing (DFM) methods are mainly developed for traditional manufacturing processes. Thus, to take full advantage of the unprecedented capability of the AM process, design for additive manufacturing (DFAM) methods need to be developed [2][3]. Typical DFAM methods include topology optimization, design for multi-scale structures (lattice or cellular structures), multi-material design, part consolidation, and other design methods which can make use of AM-enabled features. Particularly, lattice structures have many superior properties, which make it a promising solution for various applications, such as lightweight structures due to high specific stiffness and strength [4][5], heat exchangers due to large surface area [6][7], energy absorbers due to ability to undergo great deformation at a relatively low stress level, and acoustic insulators due to its large number of internal pores [8]. In addition, topology optimization is a well-established digital design tool for optimizing the distribution of material in the design domain, such that a certain objective is minimized subject to

design and response constraints.

However, there are still some problems when using lattice infill and standard topology optimization to design structures for AM. Traditional lattice structures are often of a regular or random pattern, which is selected by the user in the commercial software with a specific volume percentage or reconstruction from the CT images of the real natural object, such as bone structures. The internal structure of natural bone is a functionally graded cellular structure (FGCS) [9], and the stress distribution of a mechanical part also exhibits a variable-density form. Therefore, the functionally graded lattice structure is more reasonable for optimum structural design. Additionally, conventional topology optimization is performed only to minimize the compliance of the design while constraining the overall volume fraction to a target value. The optimized structure tends to generate a numerous of overhang structures [10], which need support structures added so that it is manufacturable. However, some support structures are difficult to remove. Further, conventional topology optimization algorithm usually solves the discrete void or solid design problem by converting the design variable that varies continuously from 0 to 1. Moreover, some isolated solid and some intermediate relative densities would be converted to 0 or 1 to produce the physically meaningful design. Besides, the optimized result needs to convert to a smoothed CAD model before it can be manufactured.

To overcome these issues, we present a generative design optimization method for the generation of stress aware functionally graded cellular structures. This approach combines the advantages of topology optimization with lattice design to further improve stiffness and manufacturability. It maximizes the mechanical stiffness by optimizing the cellular materials distribution in a given design domain and under a given external load. In particular, to generate graded cellular structures, we present a gyroid-based function representation (F-Rep) method to obtain continuous cellular structures. The smoothed result can be generated from implicit modeling algorithm directly, which can avoid computationally expensive Boolean operations of traditional lattice infill method. Also, the effective mechanical properties of the cellular structures are calculated by using computational homogenization methodology and described by anisotropic constitutive laws [11][12]. For validation purposes, the structural robustness of the optimized structures belong to various design cases are analyzed through Finite Element Analysis (FEA) and experiment further.

Specific contributions of this paper are:

- The geometric continuity and connectivity of gyroid-based cellular structure are optimized, which makes the mechanical properties of low-density is meaningful, and the density design space of gyroid structure is expanded.
- A design methodology for generating functionally graded cellular structures based on optimized gyroid structure and structure optimization is presented.
- We have demonstrated the structural effectiveness and robustness of the proposed optimization approach through several examples.

2. Related Works

In DFAM areas, much research has been focused on the optimization of geometric shapes and topology structures with specific physical properties. In this section, we review the optimization of mechanical properties techniques

related to this work.

Infill Optimization for AM: Infill optimization is not only for obtaining a lighter weight structure, but also for achieving a sufficiently large stiffness. Similar to 2D texture mapping, Chen [14] presented a 3D texture design method which maps lattice into a design space to generate internal structures, and this system is based on a microstructure library. Inspired by the construction of truss structures, Wang et al. [15] optimized the mechanical stiffness of an object by using a "skin-frame" structure to support interior of the object. Lu et al. [16] introduced a honeycomb-cell structure by gradually carving out the interior of an object, but the enclosed hollowed cells make it difficult to remove the internal supporting materials. Thus, Wang et al. [17] developed a support-free hollowing algorithm based on the method in [16]. Li et al. [18] introduced a technique to control the parameters of the microstructures so that they can vary spatially to produce graded materials. The technique is combined with a cross-sectional stress analysis method [19] to reinforce a part. Additionally, many researchers have taken manufacturability of AM into account. Wu et al. [20] proposed a rhombic cell which was self-supporting. As a concurrent work, Xie and Chen [21] suggested a similar support-free interior carving by the rhombic cell for 3D printing. Li et al. [22] developed a gyroid-based functionally graded lattice structure for buoyancy optimization and proved that the gyroid structure was self-supporting.

Gyroid Structure: The gyroid structure is discovered by NASA scientist Alan Schoen in 1970 [23], which is designed for lightweight high-strength new materials. Due to AM techniques, the geometric and mechanical properties of gyroid structures have been extensively studied. Yan et al. [24][25] used SLM (selective laser melting) method to evaluated the manufacturability and mechanical properties of gyroid lattice structures with different density, and unit cell sizes ranging from 2 to 8 mm can be manufactured without external support structures. Besides, Hussein et al. [26] and Strano et al. [27] used gyroid structure as support structures of parts for AM. Additionally, Khaderi et al. [28] analyzed the stiffness and strength of the gyroid lattice by finite element method (FEM). Yánez et al. [29] proved that gyroid titanium structures has versatile stiffness and strength to be used for correction of bone defects. Ataee et al. [30] also used gyroid structures for bone implant applications by electron beam melting (EBM).

Topology Optimization: Topology optimization is a mathematical method that optimizes material distribution within a given design space, for a given set of loads, boundary conditions and constraints with the goal of maximizing the performance of the system. The most common method is homogenization based method [31][32], solid isotropic material with penalization (SIMP) [33][34][35], level-set method [36][37], bi-directional evolutionary structural optimization (BESO) [38][39] and the various algorithms they derived. The BESO algorithm is a finite element-based topology optimization approach, where the inefficient material is iteratively removed from a structure while the efficient material is simultaneously added to the structure. The basic principle of SIMP algorithm is to calculate the evolution of relative density distribution of the elements over the design space. For a detailed description of SIMP and BESO topology optimization techniques, see the recent survey articles [40][41]. In this paper, we establish the scaling law [11][12] of an elastic matrix of the lattice structures by the homogenization theory [13]. Next, the optimal density distribution of a component is calculated by this scaling law added optimization algorithm. Besides, different from the original SIMP method, we convert the design variable to cellular structures that varies continuously from $\rho_{\min}$ to $\rho_{\max}$.

Functionally Graded Cellular Structure: FGCS is a type of functionally graded material (FGM), FGM is mainly designed by having a variable proportion of composite materials with random microstructures, while FGCS is mainly focused on the density-variable lattice or porous structures design according to the physical and mechanical properties [42]. Here we focus on discussing topology optimization based the relative density mapping approach. Brackett et al. [43] first proposed a SIMP based density mapping approach to map the intermediate densities to lattice cells of varying volume fraction in 2D. Several similar techniques [44] were proposed to optimize the cellular structures using relative density directly from the SIMP method. Song et al. [45] used irregular honeycomb cellular structure as the distribution materials. Furthermore, Zhang and Cheng et al. [46][47] took the anisotropic property of cellular materials into account by the homogenization method. Liu et al. [48] proposed a method to generate a spatially varying structure of FGM with target properties from CT image or topology optimization. Besides, Liu et al. [49] developed a two-scale structure synthesis method to generate anisotropic microstructures in the design domain. Wang et al. [50] used an efficient homogenization-based topology optimization method to generate variable-density honeycomb cellular structure for natural frequency optimization. Tang et al. [51] proposed a BESO based design method for truss-like lattice structure optimization. Daynes et al. [52] presented a combined methodology of topology optimization and size optimization. Additionally, Wu et al. [53] presented a new approach to the generation of bone-like porous structures based on topology optimization method. Moreover, the structural robustness of the optimized bone-like porous structure was discussed. The optimized porous structure was verified to have the ability to resist undefined loads and local damage. Wang et al. [54] proposed a level-set based topology optimization method to design connectable graded microstructures, and the optimized structures have good manufacturability. Chen et al. [6][7] generated the graded lattice structures to optimize the heat conduction of the object based on level set method.

3. Methodology

The proposed design methodology for cellular structure optimization mainly consists of two parts: functionally graded cellular structures design and optimization procedure, which is illustrated in the flowchart in **Fig. 1**. Firstly, for the FGCS design part, we present an implicit function to generate the gyroid structures of uniformly varying density based on the previously established relationship between the parametric equation of gyroids and the volume fraction in Section 4. Moreover, the geometric continuity and connectivity of the structure are optimized. Secondly, in this methodology, the effective mechanical properties of gyroid-based cellular structures are described by anisotropic constitutive laws. In addition, we assume that the elastic constants in the anisotropic model are exponential functions of the relative density, which are determined by using computational homogenization method. Based on a set of computational data, a formulation of relative density is proposed to represent the equivalent material properties of the specific cellular structure. In Section 5, for the optimization procedure, the penalization formulation in standard structure optimization is replaced by the fitted homogenized model. The exact relative density of a certain cell will be determined by solving the structural optimization problem. Lastly, further validation of the introduced object is conducted via experimental tests on 3D printed samples in Section 6.

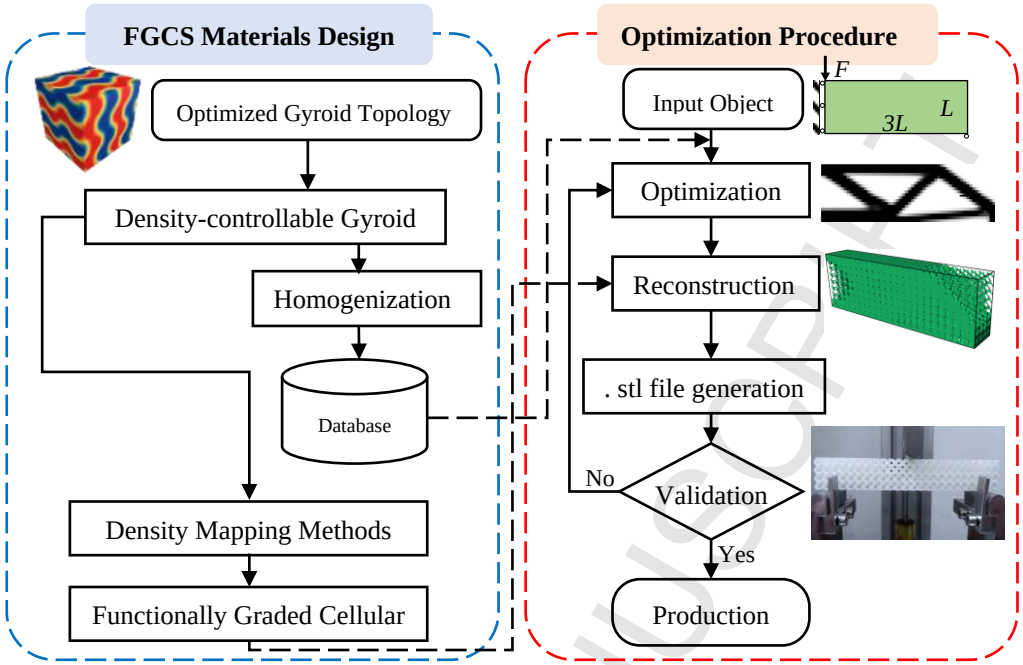

Fig. 1. Procedures for design optimization of functionally graded cellular structures (FGCS).

4. Design of Gyroid Structure

4.1. Geometric properties

Most lattice structures are made up of arrays of slender members that resemble familiar lightweight super-structures such as bridges and building frames. But not all lattice structures comprise simple strut and node arrangements. In this work, we choose gyroid structure, which is a typical triply periodic level surface (TPLS) and has been discovered to exist in nature stably. The main advantages of gyroid structure are: (1) The open-cell foam structure which enables easy removal of powder or liquid resin. (2) The self-support helical structure which does not require any supporting materials during additive manufacturing. (3) High specific surface area and low relative density while retaining higher specific strengths than regular diamond lattices in certain circumstances [55]. Furthermore, a gyroid structure has a wider connectivity area than other types of TPLS structures, such as Schwarz Diamond and Schwarz Primitive, when the level parameter is variable. All of these advantages indicate the usefulness of gyroid structures towards topological design for lattice materials.

Triply periodic level surfaces represent the solution to scalar-valued functions of three independent variables. The three independent variables can be considered as the *x*, *y*, and *z* coordinates of a point in three-dimensional Euclidean space. The equation of gyroid level surface is composed of trigonometric functions $F: R^3 \to R$ at point $(x, y, z) \in R^3$, and a close approximation to the gyroid is defined as:

$$F_{\text{Gyroid}}(x,y,z) = \sin\left(2\pi\frac{x}{L}\right)\times\cos\left(2\pi\frac{y}{L}\right) + \sin\left(2\pi\frac{y}{L}\right)\times\cos\left(2\pi\frac{z}{L}\right) + \sin\left(2\pi\frac{z}{L}\right)\times\cos\left(2\pi\frac{x}{L}\right) - t \quad (1)$$

where *L* is the cubic unit cell edge length, and the level parameter *t* is a variable and determines the volume fractions pertaining to the regions separated by the surface. The lattice structures are subjected to translation and scaling and pinched off into unconnected blobs as the value of the parameter *t* becomes sufficiently negative or

positive. A distinct advantage of using mathematical expressions to define the lattice structures is that a desired number of parameters can be assigned to the model, so that a subsequent architecture optimization for cellular materials study can be carried out with relative ease. The possible values for t and the resulting structures are discussed below:

- t = 0: The minimal gyroid surface divides space into two helical regions, each claiming a volume fraction of 50%, see **Fig. 2a**. When one of the areas is closed, a lattice structure with a volume fraction of 50% is obtained (see **Fig. 2b**).
- 0<|t|<1.41: With the increase of t, the proportions of A and B regions also monotonously increase or decrease. When t is positive, the volume fraction increases in the positive direction. When t is negative, the volume fraction decreases in the negative direction. As shown in **Fig. 2c** and **d**, it is unit cell and 3×3 cells of gyroid when t is equal to -1.31.
- |t|=1.41: For this value, the so-called "pinch-off" (i.e., disconnects) surface is generated, and the surface will be disconnected (see **Fig. 2e** and **f**). For a low density, such a structure loses its mechanical properties, and for high density, the resulting enclosed area prevents the removal of powder or liquid for AM technique.
- 1.41<|t|≤1.5: For these t values, the gyroid surface is no longer connected (see **Fig. 2g**) and will be optimized in Section 4.2. Moreover, when |t|>1.5, the surface disappears.

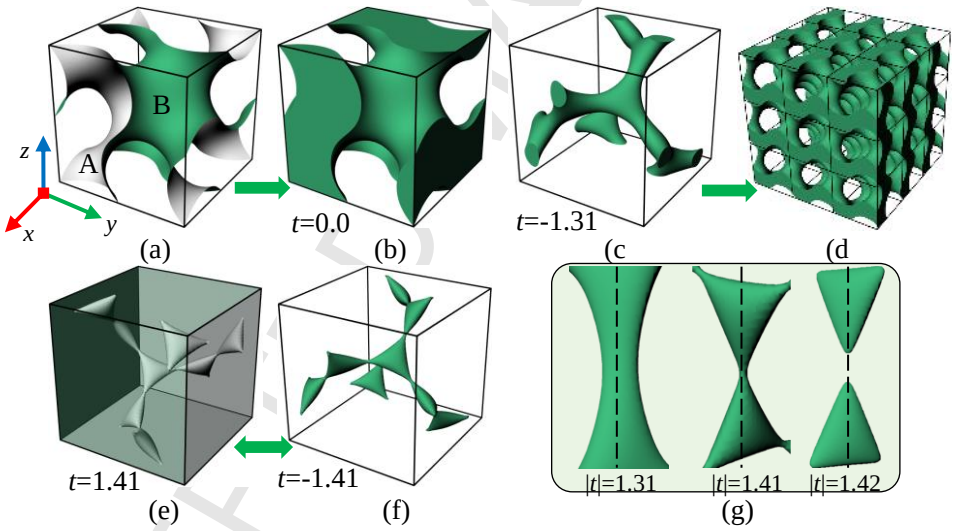

Fig. 2. Geometric properties of gyroid cellular structures with different relative densities: (a) gyroid surface, t=0.0; (b) gyroid cellular, t=0.0; (c) and (d) unit cells and array of 3×3 cells, t=-1.31; (e) and (f) pinch-off structure of gyroid, |t|=1.41; (g) struct shape with different t.

4.2. Morphological optimization

The pinch-off problem is an important flaw based on TPLS modeling. Basically, all TPLS-based cellular structures have geometric discontinuities problems. For example, the volume fractions of Schwarz Primitive and Schwarz Diamond structures are about 25% at pinch-off, and that of gyroid structure is about 10%. When the cellular is no longer continuous, not only the design space is limited, but also the broken area will make the structure fragile, and the closed cells make the manufacturability poor. The gyroid structure has been widely used because of its excellent mechanical properties and self-supporting ability when used in AM. In this work, in order to solve the pinch-off problem, the original equation is locally optimized. A penalty function is added into Eq. (1) when |t|≤1.41. Then,

the pinch-off optimized gyroid-based cellular function can be expressed as:

$$F^{*}_{Gyroid} = \begin{cases} F_{Gyroid} & , \ 0 \le |t| < 1.41 \\ F_{Gyroid} - \varphi(x,y,z), & 1.41 \le |t| \le 1.5 \end{cases} \tag{2}$$

where φ(x, y, z) is the penalty function. Since the porous structure of gyroid exhibits an approximately spherical shape, we construct a ball-shaped triple-period structure to adjust morphology of the gyroid shape. Moreover, the penalty function is expressed as:

$$\varphi(x,y,z) = (0.45*t - 0.58)*\left[cos(2x)cos(2y) + cos(2y)cos(2z) + cos(2z)cos(2x)\right] \tag{3}$$

where (0.45*t-0.58) control the punishing intensity of the shape. The larger the level parameter t is, the more severe the pinch-off is (see **Fig. 2g**), so the penalty strength needs to increase with the t value. As shown in **Fig. 3a~d** are the pinch-off optimization process. In **Fig. 3e** and **f** are the optimized morphology results with $|t|$=1.41. Compared with the original gyroid structure, the pinch-off phenomenon is disappeared. Even if $|t|$ is large, the optimized gyroid also has geometric continuity (see **Fig. g** and **h**).

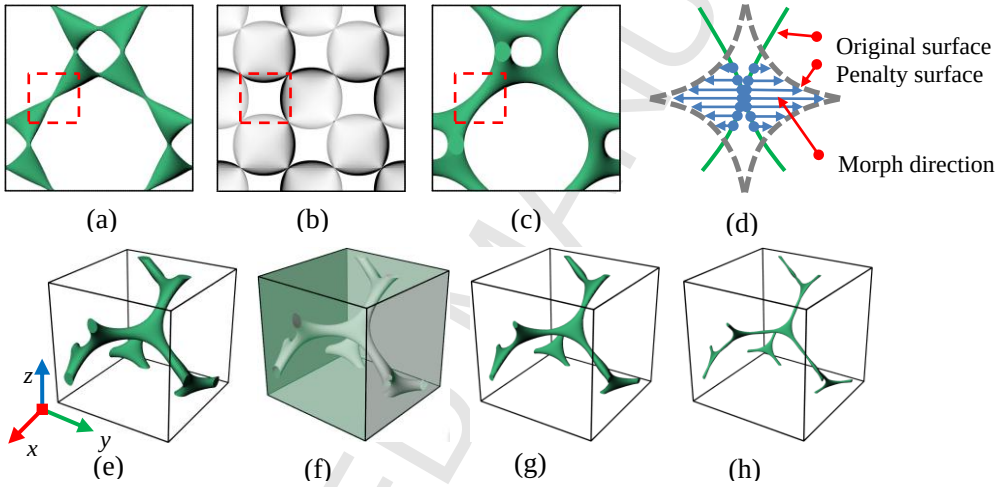

Fig. 3. Morphological optimization procedure of gyroid-based cellular structures: (a) original gyroid structure, t=-1.41; (b) constructed penalty surface; (c) and (e) optimized gyroid structure, t=-1.41; (d) demonstration of optimization process in 2D; (f) (g) and (h) optimized gyroid structures with t=1.41, t=-1.45 and t=-1.48, respectively.

The relative density, or the volume fraction of the solid phase, is an important parameter for cellular materials that is usually used as a variable to express other properties, such as elastic modulus and yield stress. It is essential to acquire the relationship between parameter t and relative density ρ_G for gyroid lattice structure. According to Eq. (2), we generate structures of different densities of gyroids and calculate their volume fractions, respectively. The data plotted in **Fig. 4** reflect how the relative density of gyroid structure changed with the level parameter t. Moreover, it shows that the relative density increases linearly with t. The best fitting of data gives the scaling laws of relative density for gyroid structure as follows:

$$\rho_G = 0.3325 \times t + 0.501 \quad , \quad |t| \le 1.5 \tag{4}$$

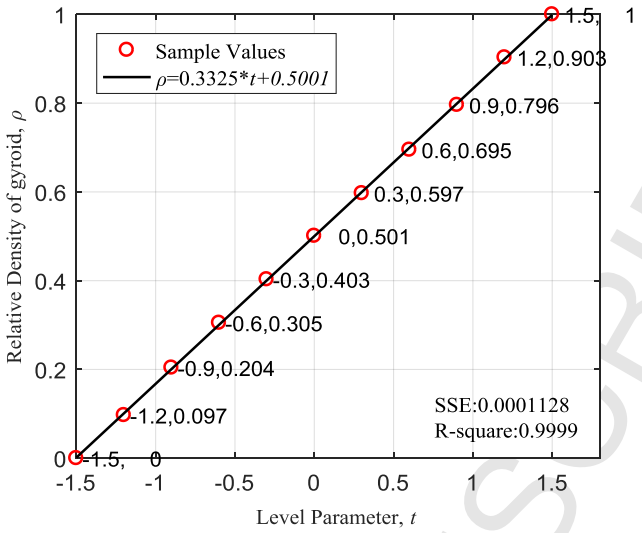

Fig. 4. Scaling laws of the relative density of gyroid-based cellular structures.

4.3. Mechanical properties

The mechanical properties of a cellular structure depend directly on the shape and topology of cells. In this work, we choose the gyroid lattice structure as the basic cell, not only because of its controllable geometrical morphology and compact mathematical expression, but also for its excellent mechanical properties. Relative density ρ_r is an important characteristic of cellular structures. According to the Gibson-Ashby model [11][12], the elastic modulus E, shear modulus G, and yield strength σ_{pl} of cellular structures are functions of the relative density. These functions are called "scaling laws". In the case of the elastic modulus E, the scaling law follows the form $E_c/E^*=f(\rho_r)$, in which E_c and E^* are elastic moduli of the cellular structure and constituent material, respectively, and $f(\rho_r)$ is a polynomial or power function of the relative density ρ_r.

The mechanical behavior of a cellular structure is generally anisotropic. According to Simone and Gibson [12], a scaling law for anisotropic cellular structures also exists. In this work, a simple and straightforward numerical homogenization technique proposed by Steven [13] is used to obtain the effective stiffness matrix of the non-continuum, periodic lattice structures. In Hooke's law, $\{\sigma\}=[C]\{\varepsilon\}$, unknow constants of the fourth-order stiffness matrix $\boldsymbol{C}$ can be reduced from 81 to 21 due to the symmetry in an orthogonal system. In numerical realization [13][58], in each step, one strain component was set to unity whereas the rest five as zero, e.g., Eq. (5).

$$\text{Input: } \begin{Bmatrix} \varepsilon_{11} \\ \varepsilon_{22} \\ \varepsilon_{33} \\ \varepsilon_{23} \\ \varepsilon_{31} \\ \varepsilon_{12} \end{Bmatrix} = \begin{Bmatrix} 1 \\ 0 \\ 0 \\ 0 \\ 0 \\ 0 \end{Bmatrix} \quad \text{Output: } \begin{Bmatrix} \sigma_{11} \\ \sigma_{22} \\ \sigma_{33} \\ \sigma_{23} \\ \sigma_{31} \\ \sigma_{12} \end{Bmatrix} = \begin{Bmatrix} C_{11} \\ C_{21} \\ C_{31} \\ C_{41} \\ C_{51} \\ C_{61} \end{Bmatrix} \tag{5}$$

In the process, the unit strain is represented as a specified displacement on the boundary. Therefore, the corresponding stresses can be calculated by the reaction forces in FEA. The stiffness matrix of a cellular structure is determined by six FEA. There are two types of strains: normal strain and shear strain, which correspond to the two

forms of boundary conditions. Take the normal strain ε_x (ε_{11}) in the x-axis direction as an example, the boundary conditions are defined as:

$$\begin{aligned}&\Delta l_x\big|_{x=l_x}=0.001l_x\\&\Delta l_x\big|_{x=0}=\Delta l_y\big|_{y=l_y}=\Delta l_y\big|_{y=0}=\Delta l_z\big|_{z=l_z}=\Delta l_z\big|_{z=0}=0\end{aligned}\tag{6}$$

which means that when $x=l_x$, i.e., ε_x =0.001, the displacement in the x-axis direction is $0.001l_x$, and the displacements of rest directions are zeros. Take a shear strain γ_{xy} (ε_{12}) for example, and the boundary conditions are expressed as:

$$\begin{aligned}&\Delta l_x\big|_{z=l_x}=0.0005l_z,\ \Delta l_z\big|_{x=l_z}=0.0005l_x\\&\Delta l_z\big|_{x=0}=\Delta l_y\big|_{y=l_y}=\Delta l_y\big|_{y=0}=\Delta l_z\big|_{z=l_z}=\Delta l_x\big|_{z=0}=0\end{aligned}\tag{7}$$

The definition of boundary conditions for the other normal strains and shear strains are similar to the above ones. The complete homogenization procedure is programmed in Python language with the FEA of each numerical experiment implemented in ABAQUS. To the calculated results, it is found that the gyroid-based cellular structures belong to a cubic symmetric system. Therefore, in the matrix $\boldsymbol{C}_{\mathrm{TPLS}}$: $C_{11}=C_{22}=C_{33}$, $C_{12}=C_{13}=C_{23}$, $C_{44}=C_{55}=C_{66}$ and other constants are zero.

$$\boldsymbol{C}_G=\begin{bmatrix}C_{11}&C_{12}&C_{12}&0&0&0\\C_{12}&C_{11}&C_{12}&0&0&0\\C_{12}&C_{12}&C_{11}&0&0&0\\0&0&0&C_{44}&0&0\\0&0&0&0&C_{44}&0\\0&0&0&0&0&C_{44}\end{bmatrix}\tag{8}$$

To find the elastic scaling laws of the gyroid cellular structures, an exponential function is fitted to the computational result to figure the relationship between constants of the elastic matrix and relative density of cellular. In structure optimization procedure, the elastic scaling laws become 1 when ρ_{r} is 1 and become 0 when ρ_{r} is 0. Therefore, the fitted function passes two points: (1,1), (0,0). To the exponential function form, the elastic scaling laws of lattice structures can be expressed as:

$$\boldsymbol{C}_G\left(\rho_r\right)=\boldsymbol{a}_1e^{\boldsymbol{a}_2*\rho_r}-\boldsymbol{a}_1\tag{9}$$

where $\boldsymbol{a}_1$, $\boldsymbol{a}_2$ are the constant symmetric matrices. They are obtained after fitting to the FEA simulation results. For the gyroid structure, the scaling laws for the three independent material constants obtained after fitting to the finite element simulation data are found to be:

$$\begin{aligned}&C_{11}/C_{11}^*=0.0605e^{2.8659*\rho_r}-0.0605\\&C_{12}/C_{12}^*=0.0396e^{3.2513*\rho_r}-0.0396\\&C_{44}/C_{44}^*=0.1452e^{2.0729*\rho_r}-0.1452\end{aligned}\tag{10}$$

where C_{11}^*, C_{12}^* and C_{44}^* are corresponding elastic constants of the composing material. Moreover, the fitting result is plotted in **Fig. 5a**.

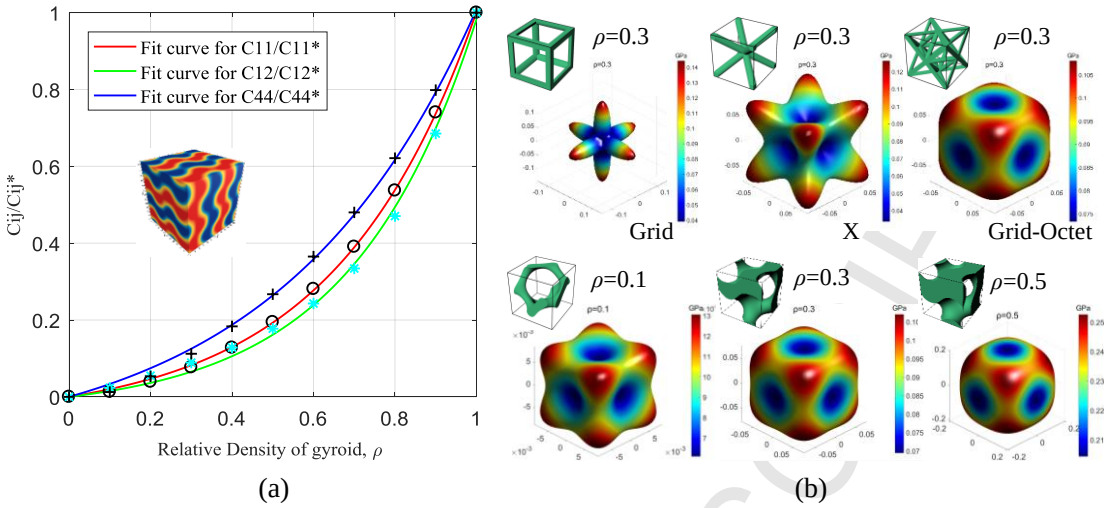

Fig. 5. Mechanical properties of gyroid structure calculated by homogenization method: (a) elastic scaling law for gyroid structure; (b) 3D spatial representations of effective Young's modulus surfaces.

According to computational homogenization methodology presented by Steven [13], the effective stiffness matrix of gyroid-based unit cells and three typical frame-based lattice structures are evaluated. Plotting Young's modulus surface in an orthogonal coordinate system similar to the method for analyzing the elastic anisotropy of monocrystalline [59], the strong and weak directions can be demonstrated in **Fig. 5b~g**. The elastic anisotropy of lattice structures is highly dependent on the volume fraction. From the result, it can be seen that Young's modulus of Grid lattice and X lattice have significant changes along with different directions. However, gyroid and Grid-Octet lattice structures have less variation along with different directions. In addition, stress analysis is performed in the z-axis direction as shown in **Fig. 6**. It shows that stress is concentrated on the connections of Gird, X and Grid-Octet lattices in directions parallel to the loading direction as the compressive loading is applied. In case of gyroid lattice structure, the surface and nodes are smooth, when the loading is applied to the structure, the stress concentration phenomenon is less than other types of lattice structures. Thus, this material property enables the optimized design to cope with uncertain external loads without significant variations in stiffness.

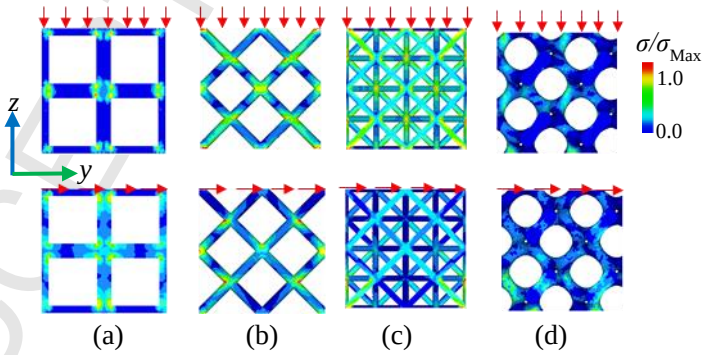

Fig. 6. Stress distributions of Grid, X, Grid-Octet and gyroid structures under compressive loading along the z-direction and shear loading along the x-direction, respectively. For visualization, the stress is normalized by the maximum stress.

5. Design of Functional Graded Cellular Structure

5.1. Properties mapping

In this work, to realize continuous density variable gyroid lattice structure in 3D space, the level parameter t is modified as a continuous function: $t(x,y,z)$ in R^3, and then the functionally graded gyroid lattice structure can be expressed as:

$$\bar{F}_{Gyroid}(x,y,z)=F^{*}_{Gyroid}-t(x,y,z) \tag{11}$$

In this function, $t(x,y,z)$ is the density of a certain point $(x,y,z)\in R^3$ which can be represented with an expression of high degree to achieve more complex density distribution. If the material density function $\rho_{\text{Material}}(x,y,z)$ is a continuous function (can be material properties such as stress, Young's modulus, and heat distribution), $t(x,y,z)$ is also a continuous spatial function. Then we can obtain a continuous gyroid lattice structure in 3D space. For example, by giving the unit cell size L=1, x, $y\in$[-5, 5], $z\in$[-2.5, 2.5] and defining the material density function is shown in **Fig. 7a**. According to Eq. (4), the inverse scaling laws $t(x,y,z)$ can be written as:

$$t(x,y,z)=\left(\rho_{\text{Material}}(x,y,z)-0.5\right)\times 3,\quad 0\le\rho_{\text{Material}}\le 1 \tag{12}$$

As shown in **Fig. 7b**, a complex functionally graded gyroid lattice structure is generated by implicit surface reconstruction algorithm in 3D space, which maps the corresponding material properties perfectly. It is manufacturable by using 3D printing technique from density very low (3%) to very high (100%). As shown in **Fig. 7c**, the mapping result is manufacturable by using Stereolithography (SLA) 3D printing technology. In the next step, the proposed parametric gyroid lattice generation algorithm will be combined with structure optimization techniques.

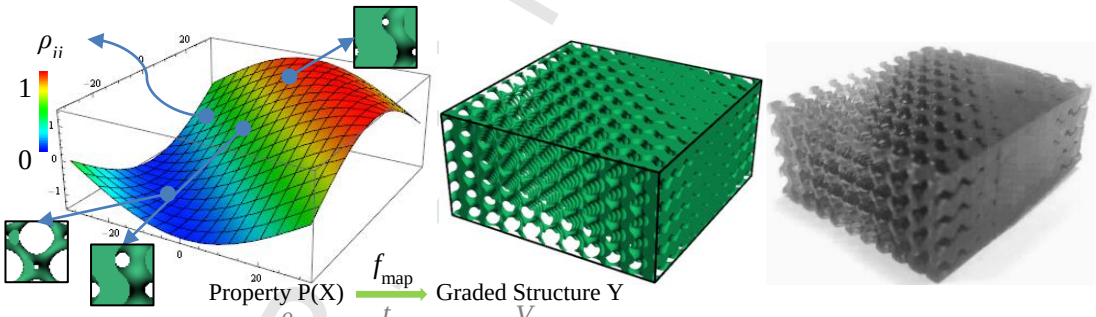

Fig. 7. Example of mechanical properties mapping process and its manufacturability verification by 3D printing: (a) material properties diagram; (b) 3D mapping result; (c) 3D printing result.

5.2. Optimization process

In this section, we discuss how to use the elastic scaling law to obtain the minimum compliance cellular structure for a mechanical component. As the effective mechanical properties can be represented through the scaling law as a function of the relative density of a given cellular structure, the relative density is treated as a design variable in our optimization process. Standard topology optimization methods such as SIMP and BESO provide an optimum solution for placing available material within a given design space to obtain best structural performance. The elements are considered as isotropic materials. It is reasonable to use the element density calculated directly by structure optimization as the basis for lattice filling, because almost all types of lattice structures are anisotropic.

Therefore, the lattice infill optimization problem can be treated as optimize density distribution of a mechanical part.

In this paper, a modified density-based topology optimization algorithm is proposed to optimize the infilling process by considering the materials properties of cellular structures. The objective function used here is to identify the optimal distribution of material density, subjected to target volume constraint, to minimize structural compliance. Hence, the mathematic expression of the minimum compliance problem for the cellular structure takes the following form:

$$\begin{aligned} &\min c(\rho_r) = \frac{1}{2}\mathbf{u}^T\mathbf{K}(\rho_r)\mathbf{u} \\ &s.t.\ \ \mathbf{f} = \mathbf{K}(\rho_r)\mathbf{u} \\ &\quad \mathbf{C}_G = \mathbf{C}_G(\rho_r) \\ &\quad V^* = \sum_{i=1}^{n} v_i \rho_r \\ &\quad 0 \le \rho_{\min} \le \rho_r \le \rho_{\max} \le 1 \end{aligned} \tag{13}$$

Where structural compliance $c(\rho_r)$ is the objective function, **K** is the global stiffness matrix, **f** is the external load vector, **u** is the displacement vector. The first constraint is the equilibrium equation. The second constraint is the elastic scaling law as discussed in Section 4. The third constraint limits the total design volume to V^*. The final constraint requires that the relative density is bounded by the minimum and maximum relative densities. Compared with the standard minimum compliance problem, the second constraint is a fictitious elastic scaling law used to drive the design variable to be void or solid during the optimization process, os it has no real physical meaning. In contrast, in the proposed approach for cellular structure design, the second constraint uses the elastic scaling law that represents the real mechanical properties of the underlying cellular structure as a function of its relative density. Hence, the intermediate densities can be achieved by the corresponding densities of cellular structures.

Besides, for the case where the external shape does not need to be retained, we can optimize the spatial lattice structure according to the printing direction further. **Fig. 8a** illustrates a given design space with boundary conditions, load, and the direction for 3D printing. According to Eq. (13), we perform an initial optimization process. The density calculated result is shown in **Fig. 8b** and the mapping result is shown in **Fig. 8c**, and it is called "Shape-retained FGCS optimization" method in this paper. Then, according to the given 3D printing direction, we remove the upper layer of the low-density area, and the underlayer low-density area is retained as support structures for AM, as shown in **Fig. 8d**. Lastly, we need to re-iterate the optimization equation based on the target volume fraction, and the new design is shown in **Fig. 8e** and **f** and the volume constraint are modified as $V^* = \sum_{j=1}^{m} v_j \rho_r$, where m is the number of elements of new design area Ω_{new}. This method is called "Direction-constrained FGCS optimization" in this paper.

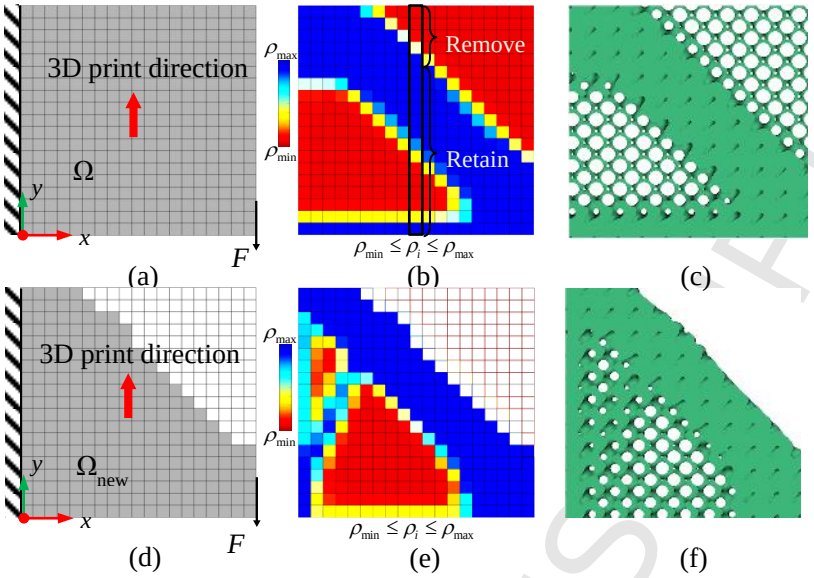

Fig. 8. Optimization process: (a) initial design space and boundary conditions; (b) and (c) shape-retained optimized result; (d) new design space; (e) and (f) 3D printing direction constrained optimized result.

6. Experimental Validation

The proposed infill optimization methodology in 3D is programmed on MATLAB code. The resulting distributed functionally graded cellular structures are lightweight, highly resistant, robust concerning uncertain force. For illustrating the effectiveness of presented optimum design methodology, both FEA simulation and experiments with 3D printed parts are conducted, and an application for quadcopter arm optimization is illustrated.

6.1. MBB experiment

To demonstrate the effectiveness of the proposed method, the classic MBB (Messerschmitt-Bölkow-Blohm) beam design problem is solved. **Fig. 9a** shows that the dimensions of the beam model are 120mm×20mm×20mm. In the model, a vertical displacement is applied onto the middle of the upper face of the beam. Displacements are fixed at the supports located at the left and right bottom face as indicated in **Fig. 9a**. Since the MBB structure is symmetrical, only the right side is selected for analysis and illustration in this paper. The finite element mesh of the half MBB beam consists of 24,000 8-noded hexahedron elements with an average element size of 1.0mm. The values used for the various materials parameters are as follows: E=2,100MPa for Young's modulus, v=0.3 for Poisson's ratio, which are the properties of the material that we are going used for 3D printing. The scaling law of the gyroid lattice structure used for optimization is given in Eq. (13), and the target volume fraction is set to 0.3. In addition, the minimum and maximum relative densities are set as ρ_{min}=0.1 and ρ_{max}=0.8. **Fig. 9b~e** shows the optimized results of different optimization strategies. We can see that the standard topology optimized results need much more support structures for AM (see **Fig. 9c**).

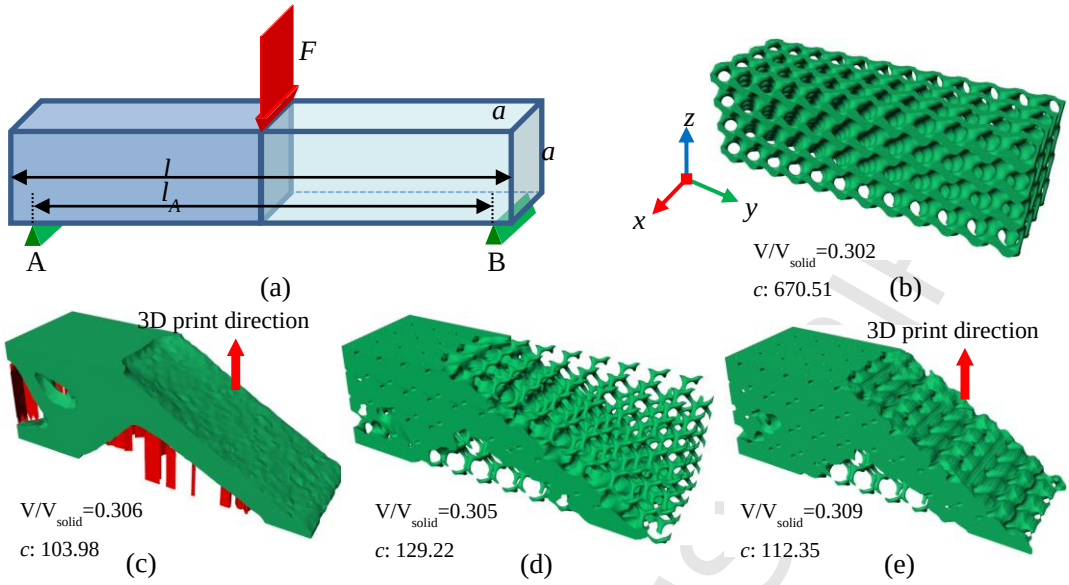

Fig. 9. Different optimization strategies of MBB beam: (a) load and boundary condition of MBB beam; (b) traditional lattice design method with uniform gyroid; (c) standard topology optimization approach; (d) our shape-retained FGCS optimization method; (e) our direction-constrained FGCS optimization method.

To conduct the FEA simulation, four types of optimization strategies were considered: the uniform gyroid lattice, standard topology optimization, our shape-retained FGCS optimization and direction-constrained FGCS optimization method, with a beam meshed using 4,888,372 tetrahedral elements (1,076,245 nodes), 3,467,928 elements (645,632 nodes), 4,590,950 elements (957,479 nodes) and 5,484,106 elements (1,078,202 nodes), respectively. The material properties used are identical to those used in the optimization, where E=2,100 MPa and v=0.3. The FEA simulation process is performed using OptiStruct 2017 software. The displacement and stress contour results are as shown in **Fig. 10**. Then, **Fig. 11** illustrates the stiffness of four designs from four different optimization strategies. From the results, it can be seen that the standard topology optimization, shape-retained FGCS optimization, and direction-constrained FGCS optimization method produces stiffer design than the uniform gyroid lattice. Under the same loading conditions, the deformation of design from direction-constrained FGCS optimization method is one-ninth of that of the uniform structure, which is very close to standard topology optimization method.

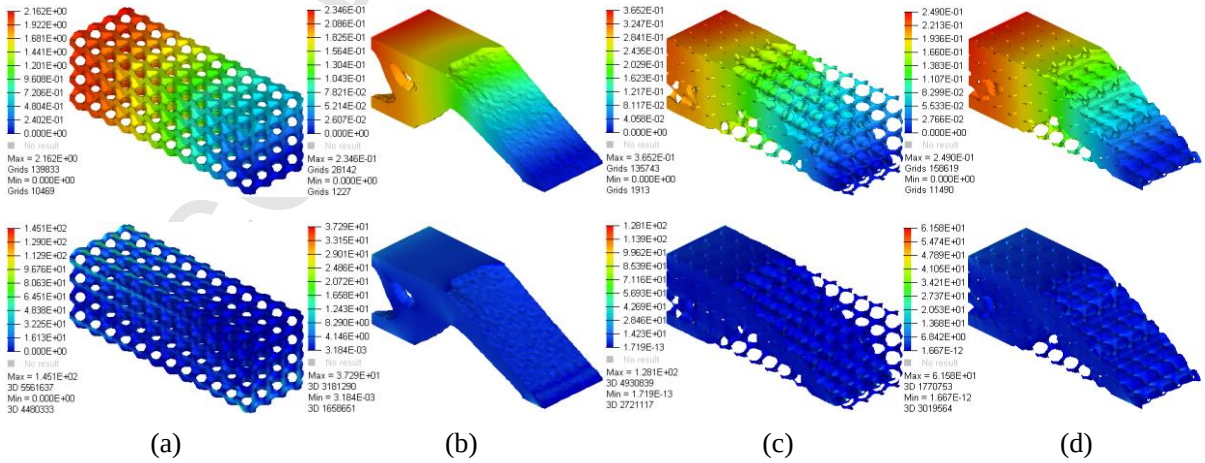

Fig. 10. Comparison different optimization strategies with the displacement and stress contour results: (a) the uniform gyroid lattice; (b) standard topology optimization; (c) shape-retained FGCS optimization; (d)

direction-constrained FGCS optimization.

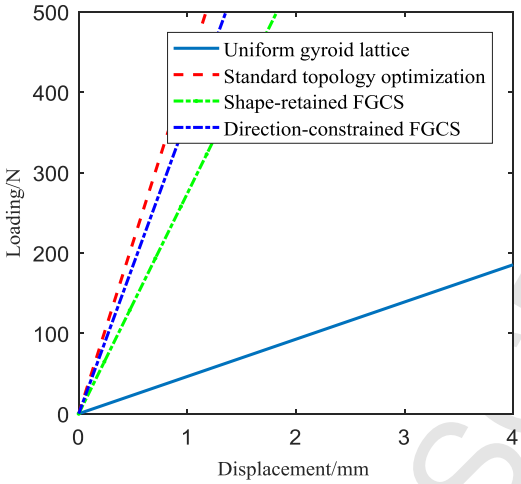

Fig. 11. Load-displacement relationships from FEA simulations of MBB beam.

For the three-point bending experiment, a full-scale uniform gyroid lattice and an optimized beam from our shape-retained FGCS optimization method are printed with a Form-2 3D Printer (formlabs Inc). The experiment on the 3D printed beams are conducted on a three-point bending setting on a loading frame, as shown in **Fig. 12a**. The beams are loaded at a rate of 0.25 mm/s until failure. The data acquisition system records the displacements and the corresponding loads. Then, we compare the experimental results between the uniform gyroid lattice and the beam from shape-retained FGCS method, which the load-displacement curves are shown in **Fig. 12b**. Note that the optimized beam is much stiffer than the uniform beam as it should be because the former is optimized for minimum compliance. Besides, the strength of the optimized beam is also 161.9 percent higher than the uniform lattice beam. These results show the effectiveness of the proposed optimization method for designing functionally graded lattice structures.

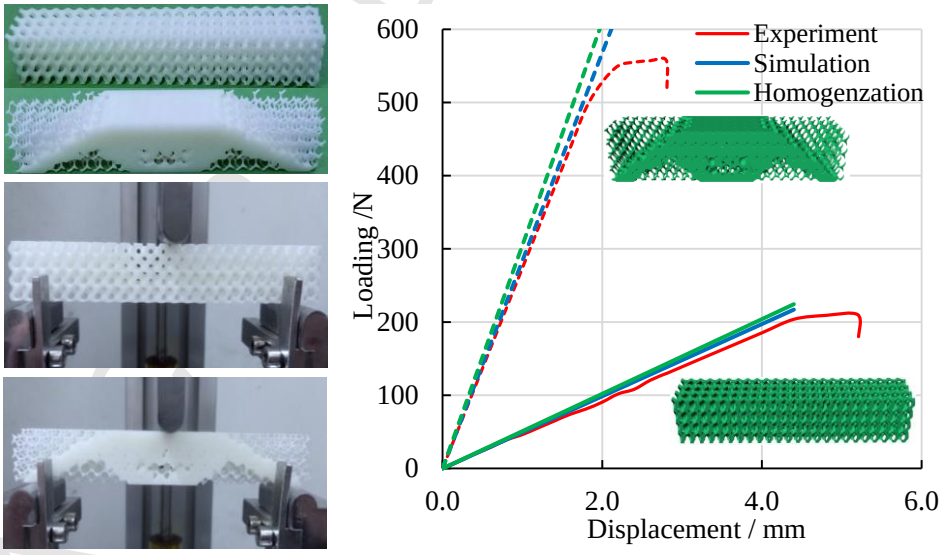

Fig. 12. Experiment for MBB beam: (a) 3D printed results and three-point bending tests; (b) load-displacement curves from three-point bending tests.

6.2. Structural robustness

Inspired by the discussion in [53], the structural robustness of the ability to withstand forces variations is discussed in this section. The advantage of the cellular structure is the ability to withstand forces from indefinite directions. Some parts are vulnerable to collisions originating from unknown directions in the actual working environment, such as quadrotors. To demonstrate this, a case of rectangular block design area is given in this section, and the boundary conditions are as shown in **Fig. 13a**. The material properties are set as: E=2,100MPa, v=0.30. As well as the target volume fraction is set to 0.3. The minimum and maximum densities are set as ρ_{min}=0.1, ρ_{max}=0.8. Then, we conduct the proposed infill optimization method to generate a functionally graded cellular structure of the design area. **Fig. 13a** shows the results of three types of optimization strategies: (a) standard topology optimization method, (b) our shape-retained FGCS optimization method, and (c) uniform gyroid cellular infill method.

To examine the effectiveness of displacement for different loading directions, we then rotate the force directions start from an initial position, and 15 degrees per rotation. Then, we reanalyze the displacement of the object under the new force direction. The displacement values in the direction of the force changes are expressed in **Fig.13b**. At the initial angle of zero degrees, displacements of the three methods are close, and the standard topology optimization and our FGCS method are better than the uniform gyroid at all angles. At angles up to about 20°, the stiffness of the standard topology optimization is higher than other methods. Then, beyond 20° our proposed method becomes better than standard topology optimization method. The above results suggest that the proposed method is able to withstand the occurrence of uncertain loads. For example, the aircraft is prone to some collision in an uncertain direction.

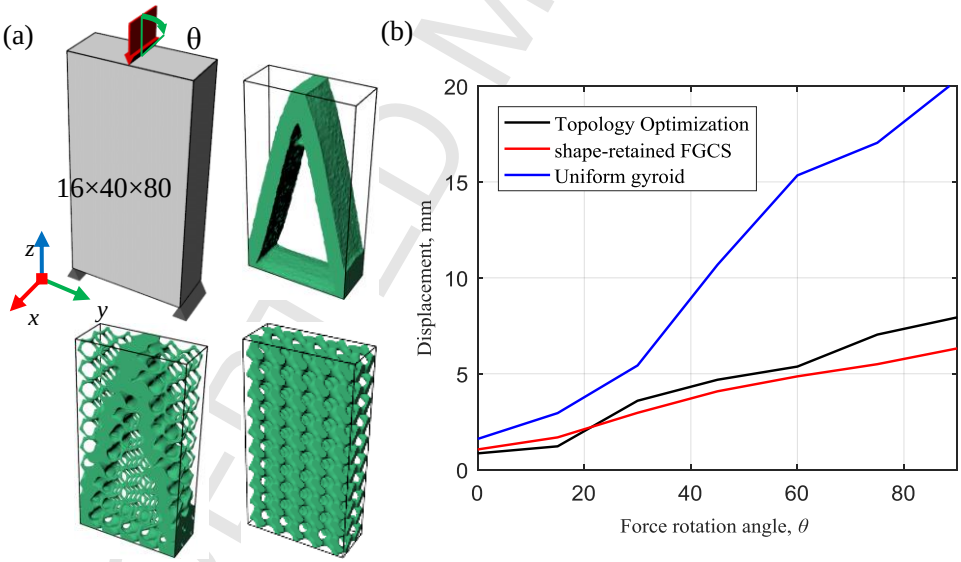

Fig. 13. Influence of force variation: (a) boundary conditions and different design strategies; (b) the displacement with respect to changing force directions of the models.

6.3. Application: quadcopter arm optimization

To further illustrate the proposed design optimization method, a design case of the quadcopter arm is given in this section. As shown in **Fig. 14a**, the arm can be simplified as a cantilever beam model with a fixed boundary condition on the left-hand side and an upward lifting force on the right-hand side from the rotating motor. The primary function of the arm is to transfer the lifting force from the propeller to the frame of the quadcopter. There

are four design requirements which are summarized based on general design and fabrication guidelines of the quadcopter [60], which are listed below.

(1) The maximum displacement at point B should be smaller than 7mm under the given load condition.
(2) The maximum stress should be smaller than the yield stress of selected materials.
(3) The total weight of the part should be small or equal to 33 g.
(4) The main body of the frame should be porous to minimize the drag force when the air passes through it vertically.

The quadrotor cantilever is most commonly designed as a truss structure. In this work, we will compare it with our proposed method by the finite element analysis simulation and the experiments on 3D printed prototypes. In our experiment, we select ABS (Acrylonitrile-butadiene-styrene) as the material for the simulation, optimization, and 3D printing. The material properties are as follows: E=2,070MPa for Young's modulus, v=0.35 for Poisson's ratio, yield stress 38Mpa. In addition, the target volume fraction is set to 0.2, and the minimum and maximum densities are set as ρ_{min}=0.1, ρ_{max}=0.8. **Fig. 14b~d** show the results of three types of optimization strategies: standard topology optimization, traditional truss design method and our FGCS based optimization method.

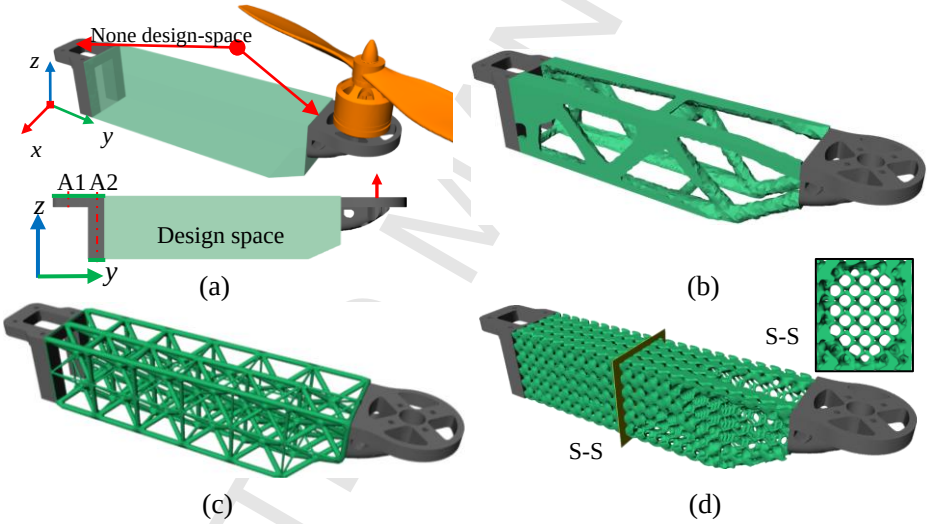

Fig. 14. Optimization results of quadcopter's arm: (a) initial shape of the arm of quadcopter; (b) standard topology optimization result; (c) traditional truss design result; (d) our FGCS based optimization result.

According to the given boundary conditions and loading conditions, the FEA simulation and topology optimization are carried out. Shown in **Fig. 15a** and **c** are the displacement contours of the truss design method and our FGCS based optimization method. It is found that the displacement of the optimized quadcopter arm is 44.7 percent less than that of the traditional truss design for the same boundary and loading conditions. To further verify this conclusion, physical tests on both truss design method and our FGCS optimization method have been carried. **Fig. 15e** shows the two optimized parts printed by a fused deposition modeling (FDM) machine (MakerBot Replicator 2X). In the physical tests, a tensile test machine (ADMET MicroEP series with a 50N load cell) is used to apply the given load and measure the displacement at the end of the arm. A clamp is used to fix the other end of the arm. The experimental setup used in this work is indicated in **Fig. 15f**. The results of FEA simulations and physical tests are summarized in **Table 1**. Both simulation and experimental data show a clear trend that our FGCS based optimization method can significantly improve the structural stiffness compared to the original truss design

method.

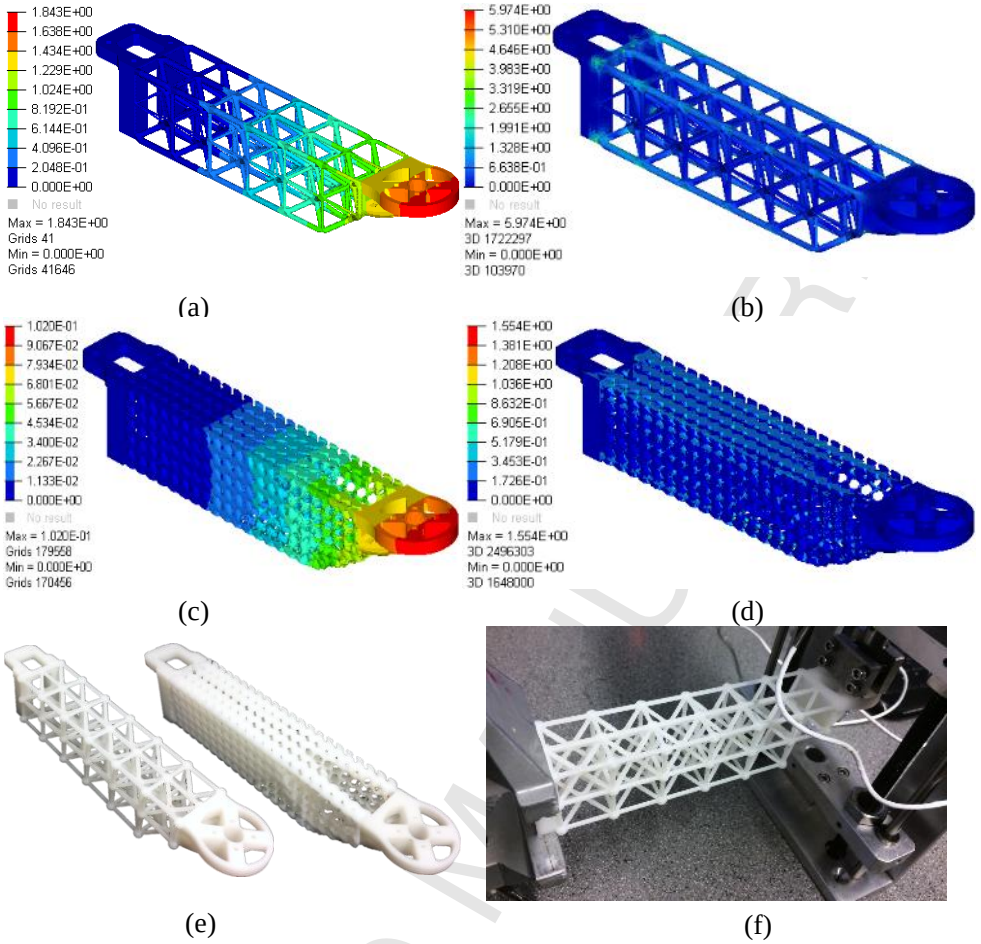

Fig. 15. Simulation and experience process of optimized results: (a) and (b) displacement and stress contour of traditional truss design method; (b) displacement and stress contour of our FGCS based optimized design method; (c) 3D printed prototypes; (d) setup of physical test.

Table 1 Results of simulation and physical tests of quadcopter's arm

Method	Volume fraction (%)	Displacement at point B (mm)		Max von Mises stress from simulation (MPa)	Manufacturability
		Simulation	Physical test		
Truss design	20.08	1.843	2.105	5.974	Need some support structures
Our FGCS optimization	20.11	1.020	1.187	1.554	Self-supporting

7. Conclusions

In this work, a method combining the functionally graded gyroid structure design with topology optimization is proposed to optimize the parts for additive manufacturing. In contrast to traditional uniform lattice design and standard topology optimization, our method not only optimizes the stiffness of the structure, but also makes the optimization result manufacturable by 3D printing. Based on the research in this paper, the following conclusions

can be drawn:

1) The "pinch-off" problem of gyroid shape is solved. Therefore, the geometric continuity and connectivity of gyroid-based cellular structures are optimized, which makes the mechanical properties of low-density is meaningful, high-density is manufacturable for AM, and the density design space of the structure is expanded.
2) A modified density-based topology optimization strategy is used to find the optimum density distribution of cellular structures. Moreover, the scaling law of material properties of the gyroid-based cellular structure is obtained by using homogenization method, and it is added to the optimization process.
3) We have demonstrated the effectiveness and robustness of our proposed optimization approach through several examples numerically and experimentally.

As the future work, we will extend the approach to multi-physics structural optimization by considering other important factors such as temperature gradient and heat transfer.

Acknowledgment

This work was supported by National Science Foundation of China (Grant No. 51775273); Natural Science Foundation of Jiangsu Province, China (No. BK20161487); Six talent peaks project in Jiangsu Province,China(Grant No. GDZB-034); Postgraduate Research & Practice Innovation Program of Jiangsu Province (Grant No. KYKX16_0320); Financial Support from the Program of China Scholarships Council (No. 201706830039).

References

[1] Gao W, Zhang Y, Ramanujan D, et al. The status, challenges, and future of additive manufacturing in engineering[J]. Computer-Aided Design, 2015, 69: 65-89.

[2] Thompson MK, Moroni G, Vaneker T, Fadel G, Campbell RI, Gibson I, Bernard A, Schulz J, Graf P, Ahuja B, Martina F. Design for Additive Manufacturing: Trends, opportunities, considerations, and constraints. CIRP Annals-Manufacturing Technology 2016; 65(2):737-760.

[3] Tang Y, Zhao YF. A survey of the design methods for additive manufacturing to improve functional performance. Rapid Prototyping Journal 2016; 22(3):569-590.

[4] Evans AG, Hutchinson JW, Fleck NA, Ashby MF, Wadley HNG. The topological design of multifunctional cellular metals. Progress in Materials Science 2001; 46(3):309-327.

[5] Wadley HNG. Multifunctional periodic cellular metals. Philosophical Transactions of the Royal Society of London A: Mathematical, Physical and Engineering Sciences 2006; 364(1838):31-68.

[6] Cheng L, Liu J, Liang X, et al. Coupling lattice structure topology optimization with design-dependent feature evolution for additive manufactured heat conduction design[J]. Computer Methods in Applied Mechanics and Engineering, 2018.

[7] Cheng L, Liu J, To A C. Concurrent lattice infill with feature evolution optimization for additive manufactured heat conduction design[J]. Structural and Multidisciplinary Optimization, 2018: 1-25.

[8] Tao W, Leu MC. Design of lattice structure for additive manufacturing. Flexible Automation (ISFA), International Symposium on. IEEE 2016; 325-332.

[9] Schaedler TA, Carter WB. Architected cellular materials. Annual Review of Materials Research 2016; 46:187-210.

[10] Kuo YH, Cheng CC, Lin YS, San CH. Support structure design in additive manufacturing based on topology optimization. Structural and Multidisciplinary Optimization 2018; 57(1):183-195.

[11] Ashby MF. The properties of foams and lattices. Philosophical Transactions of the Royal Society of London A: Mathematical, Physical and Engineering Sciences 2006; 364(1838):15-30.

[12] Simone AE, Gibson LJ. The effects of cell face curvature and corrugations on the stiffness and strength of metallic foams. Acta Materialia 1998; 46(11):3929-3935.

[13] Steven GP. Homogenization of multicomponent composite orthotropic materials using FEA. International Journal for Numerical Methods in Biomedical Engineering 1997; 13(7):517-531.

[14] Chen Y. 3D texture mapping for rapid manufacturing. Computer-Aided Design and Applications 2007; 4(6):761-771.

[15] Wang W, Wang TY, Yang Z, Liu L, Tong X, Tong W, Deng J, Chen F, Liu X. Cost-effective printing of 3D objects with skin-frame structures. ACM Transactions on Graphics (TOG) 2013; 32(6):177.

[16] Lu L, Sharf A, Zhao H, Wei Y, Fan Q, Chen X, Savoye Y, Tu C, Cohen-Or D, Chen B. Build-to-last: strength to weight 3D printed objects. ACM Transactions on Graphics (TOG) 2014; 33(4):97.

[17] Wang W, Liu YJ, Wu J, Tian S, Wang CC, Liu L, Liu X. Support-Free Hollowing. IEEE Transactions on Visualization and Computer Graphics 2017; 1-1.

[18] Li D, Dai N, Jiang X, Chen X. Interior structural optimization based on the density-variable shape modeling of 3D printed objects. The International Journal of Advanced Manufacturing Technology 2016; 83(9-12):1627-1635.

[19] Umetani N, Schmidt R. Cross-sectional structural analysis for 3D printing optimization. SIGGRAPH Asia Technical Briefs 2013; 5:1-5:4.

[20] Wu J, Wang CCL, Zhang X, Zhang X, Westermann R. Self-supporting rhombic infill structures for additive manufacturing. Computer-Aided Design 2016; 80:32-42.

[21] Xie Y, Chen X. Support-free interior carving for 3D printing. Visual Informatics 2017; 1(1):9-15.

[22] Li D, Dai N, Zhou X, Huang R, Liao W. Self-supporting interior structures modeling for buoyancy optimization of computational fabrication. The International Journal of Advanced Manufacturing Technology 2017; 1-10.

[23] Schoen A H. Infinite periodic minimal surfaces without self-intersections[J]. 1970.

[24] Yan C, Hao L, Hussein A, et al. Evaluations of cellular lattice structures manufactured using selective laser melting[J]. International Journal of Machine Tools and Manufacture, 2012, 62: 32-38.

[25] Yan C, Hao L, Hussein A, et al. Advanced lightweight 316L stainless steel cellular lattice structures fabricated via selective laser melting[J]. Materials & Design, 2014, 55: 533-541.

[26] Hussein A, Hao L, Yan C, et al. Advanced lattice support structures for metal additive manufacturing[J]. Journal of Materials Processing Technology, 2013, 213(7): 1019-1026.

[27] Strano G, Hao L. Everson RM, Evans KE. A new approach to the design and optimisation of support structures in additive manufacturing. The International Journal of Advanced Manufacturing Technology 2013; 1-8.

[28] Khaderi S N, Deshpande V S, Fleck N A. The stiffness and strength of the gyroid lattice[J]. International Journal of Solids and Structures, 2014, 51(23-24): 3866-3877.

[29] Yánez A, Cuadrado A, Martel O, et al. Gyroid porous titanium structures: A versatile solution to be used as scaffolds in bone defect reconstruction[J]. Materials & Design, 2018, 140: 21-29.

[30] Ataee A, Li Y, Fraser D, et al. Anisotropic Ti-6Al-4V gyroid scaffolds manufactured by electron beam melting (EBM) for bone implant applications[J]. Materials & Design, 2018, 137: 345-354.

[31] Bendsoe M P, Sigmund O. Topology optimization: theory, methods, and applications[M]. Springer Science & Business Media, 2013.

[32] Bendsøe M P, Kikuchi N. Generating optimal topologies in structural design using a homogenization method[J]. Computer methods in applied mechanics and engineering, 1988, 71(2): 197-224.

[33] Zhou M, Rozvany G I N. The COC algorithm, Part II: topological, geometrical and generalized shape optimization[J]. Computer Methods in Applied Mechanics and Engineering, 1991, 89(1-3): 309-336.

[34] Rozvany G I N, Zhou M, Birker T. Generalized shape optimization without homogenization[J]. Structural optimization, 1992, 4(3-4): 250-252.

[35] Rozvany G I N. A critical review of established methods of structural topology optimization[J]. Structural and multidisciplinary optimization, 2009, 37(3): 217-237.

[36] Wang M Y, Wang X, Guo D. A level set method for structural topology optimization[J]. Computer methods in applied mechanics and engineering, 2003, 192(1-2): 227-246.

[37] van Dijk N P, Maute K, Langelaar M, et al. Level-set methods for structural topology optimization: a review[J]. Structural and Multidisciplinary Optimization, 2013, 48(3): 437-472.

[38] Querin O M, Steven G P, Xie Y M. Evolutionary structural optimisation using an additive algorithm[J]. Finite Elements in Analysis and Design, 2000, 34(3-4): 291-308.

[39] Huang X, Xie Y M. Convergent and mesh-independent solutions for the bi-directional evolutionary structural optimization method[J]. Finite Elements in Analysis and Design, 2007, 43(14): 1039-1049.

[40] Sigmund O, Maute K. Topology optimization approaches, Structural and Multidisciplinary Optimization 2013; 48(6):1031-1055.

[41] Xia L, Xia Q, Huang X, Xie YM. Bi-directional evolutionary structural optimization on advanced structures and materials: a comprehensive review. Archives of Computational Methods in Engineering 2016; 1-42.

[42] Mahmoud D, Elbestawi MA. Lattice Structures and Functionally Graded Materials Applications in Additive Manufacturing of Orthopedic Implants: A Review. Journal of Manufacturing and Materials Processing 2017; 1(2):13.

[43] Brackett D, Ashcroft I, Hague R. Topology optimization for additive manufacturing. Proceedings of the solid freeform fabrication symposium 2011; 1:348-362.

[44] Alzahrani M, Choi SK, Rosen DW. Design of truss-like cellular structures using relative density mapping method. Materials & Design 2015; 85:349-360.

[45] Song GH, Jing SK, Zhao FL, Wang YD, Xing H, Zhou JT. Design Optimization of Irregular Cellular Structure for Additive Manufacturing. Chinese Journal of Mechanical Engineering 2017; 30(5):1184-1192.

[46] Zhang P, Toman J, Yu Y, Biyikli E, Kirca M, Chmielus M, To AC. Efficient design-optimization of variable-density hexagonal cellular structure by additive manufacturing: theory and validation. Journal of Manufacturing Science and Engineering 2015; 137(2):021004.

[47] Cheng L, Zhang P, Bai J, Robbins J, To A. Efficient design optimization of variable-density cellular structures for additive manufacturing: theory and experimental validation. Rapid Prototyping Journal 2017; 23(4):660-677.

[48] Liu X, Shapiro V. Sample-based design of functionally graded material structures. ASME 2016 International Design Engineering Technical Conferences and Computers and Information in Engineering Conference 2016; V02AT03A035-V02AT03A035.

[49] Liu X, Shapiro V. Sample-based synthesis of two-scale structures with anisotropy[J]. Computer-Aided Design, 2017, 90: 199-209.

[50] Wang X, Zhang P, Ludwick S, et al. Natural frequency optimization of 3D printed variable-density honeycomb structure via a homogenization-based approach[J]. Additive Manufacturing, 2017.

[51] Tang Y, Kurtz A, Zhao YF. Bidirectional Evolutionary Structural Optimization (BESO) based design method for lattice structure to be fabricated by additive manufacturing. Computer-Aided Design 2015; 69:91-101.

[52] Daynes S, Feih S, Lu WF, Wei J. Optimisation of functionally graded lattice structures using isostatic lines. Materials & Design 2017.

[53] Wu J, Aage N, Westermann R, Sigmund O. Infill Optimization for Additive Manufacturing--Approaching Bone-like Porous Structures. IEEE Transactions on Visualization and Computer Graphics 2017; 24(2):1127-1140.

[54] Wang Y, Chen F, Wang M Y. Concurrent design with connectable graded microstructures[J]. Computer Methods in Applied Mechanics and Engineering, 2017, 317: 84-101.

[55] Qin Z, Jung GS, Kang MJ, Buehler MJ. The mechanics and design of a lightweight three-dimensional graphene assembly. Science Advances 2017; 3(1):e1601536.

[56] Ashby MF. The properties of foams and lattices. Philosophical Transactions of the Royal Society of London A: Mathematical, Physical and Engineering Sciences 2006; 364(1838):15-30.

[57] Simone AE, Gibson LJ. The effects of cell face curvature and corrugations on the stiffness and strength of metallic foams. Acta Materialia 1998; 46(11):3929-3935.

[58] Xie YM, Zuo ZH, Huang X, Yang X. Predicting the effective stiffness of cellular and composite materials with self-similar hierarchical microstructures. Journal of Mechanics of Materials and Structures 2013; 8(5):341-357.

[59] Xu S, Shen J, Zhou S, Huang X, Xie YM. Design of lattice structures with controlled anisotropy. Materials & Design 2016; 93:443-447.

[60] Javir AV, Pawar K, Dhudum S, Patale N, Patil S. Design, analysis and fabrication of quadcopter. Journal of The International Association of Advanced Technology and Science 2015; 16.

Graphic abstract:

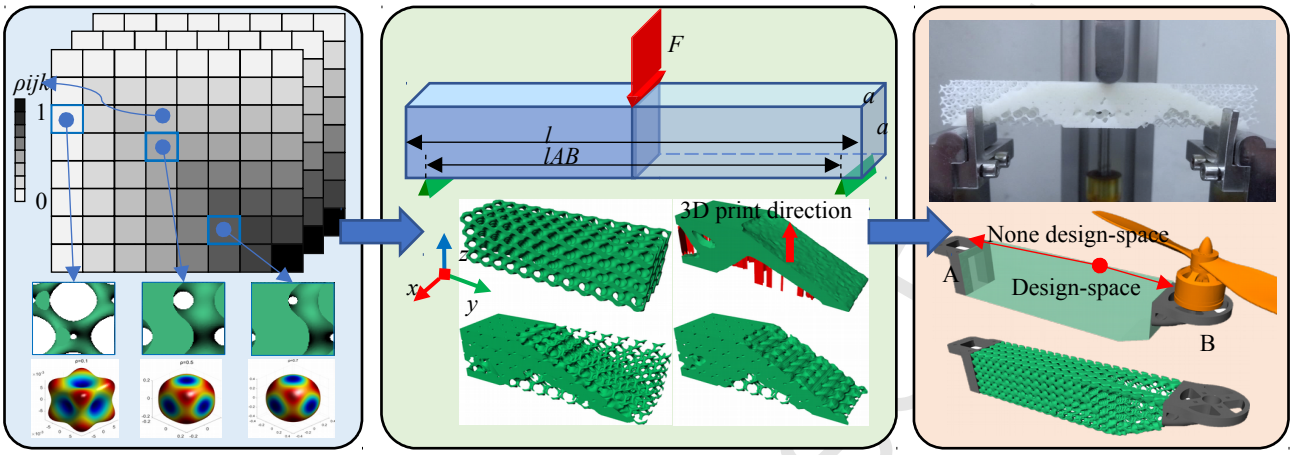

① Materials design ② Optimization strategies ③ Experiment & application

Highlights of the paper:

- The geometric continuity and connectivity of gyroid-based cellular structure are optimized, and the density design space of gyroid structure is expanded.
- A design methodology for generating functionally graded cellular structures based on optimized gyroid structure and structure optimization is presented.
- The scaling law of material properties of the gyroid cellular structure is obtained by using homogenization method, and the scaling law is added to the optimization process.